MILCOM 2024 - 2024 IEEE Military Communications Conference (MILCOM) | 979-8-3503-7423-0/24/$31.00 ©2024 IEEE | DOI: 10.1109/MILCOM61039.2024.10773912

# Design and Characterization of Dual-Band Complementary Split-Ring Resonator Array in the D-Band for 6G Wireless Networks

Laxmi Chapagain
*School of Computing*
*University of Nebraska-Lincoln*
Lincoln, NE
lchapagain2@huskers.unl.edu

Shuai Nie
*School of Computing*
*University of Nebraska-Lincoln*
Lincoln, NE
shuainie@unl.edu

***Abstract*—The D-band frequency spectrum, ranging from 110 GHz to 170 GHz, is promising in achieving high throughput in the sixth-generation (6G) wireless networks. However, efficient and low-cost antenna array designs are limited in this sub-terahertz (THz) spectrum. In this work, a complementary split-ring resonator (CSRR) antenna array is designed and analyzed. First, a single CSRR element is designed and its working mechanism is analyzed. Second, based on the element design, an array design with 2×2 elements is presented. In particular, a T-junction power divider is utilized in the feeding network. Our simulation results demonstrate that good band isolation is achieved between two resonating frequencies of 127.2 GHz and 137.8 GHz. Our designed CSRR array demonstrates a maximum gain of 13.8 dBi and 14.8 dBi at two respective resonating frequency bands. This CSRR array design with a streamlined structure has the potential for effective integration within a compact RF system, such as the sub-THz reconfigurable intelligent surfaces.**

***Index Terms*—Terahertz-band communications, antenna arrays, complementary split-ring resonator, dual-band antennas, D-band, 6G wireless networks.**

## I. Introduction

The 6G wireless networks are expected to support peak data rates of 1 terabit per second (Tbps), achieve peak spectral efficiencies of 60 bps/Hz, maintain end-to-end packet error rates as low as $10^{-9}$, and deliver end-to-end latency of 0.1 ms [1]. To achieve these ambitious goals, the D-band (110 GHz–170 GHz) has emerged as a promising frequency range for high data rate communication. Atmospheric absorption in the 125 GHz to 165 GHz range is minimal (less than 2 dB/km), further boosting its suitability for wireless applications [2]. While the D-band supports the advancement of wireless connectivity, it also introduces challenges related to path loss, transmission power, system architecture, and stringent requirements for antenna design and packaging [3].

In D-band wireless communication systems, developing compact, high-gain antennas is crucial to mitigate increased free-space path loss and ensure robust signal strength over longer distances. While dielectric lens antennas and parabolic reflectors offer high efficiency and gain, they require large RF front-end sizes due to their volumetric geometry [4]. Among different types of antenna designs, on-chip, and semiconductor-based antennas, typically fabricated using CMOS technology, are severely limited in power handling at the millimeter-wave band, restricting their applicability in high-power scenarios [4]. While capable of excellent power handling and low loss, hollow waveguide-based antenna arrays require complex 3D waveguide feed networks, which are difficult to integrate with RF circuits [4]. Substrate-integrated waveguide (SIW) antennas under printed circuit board (PCB)-based antennas, lead to complex electromagnetic behavior, requiring careful design to ensure proper mode propagation. The fabrication involves precise drilling or etching via holes to form the waveguide structure, necessitating advanced manufacturing processes and equipment, which increases fabrication costs. Low-temperature co-fired ceramics (LTCC) antennas under PCB-based antennas involve multilayer integration, adding to the design complexity. The fabrication cost is also high due to the specific materials and processes required [5].

Addressing the above-explained challenges of SIW and LTCC antennas under PCB-based antennas, our designed complementary split ring resonator antenna for D-band offers a low-profile, electrically thin, and lightweight solution. It allows for easy fabrication and integration with other active and passive microwave components similar to that of patch antenna [4]. Specifically, our technical contributions include:

- Our design of the 2×2 Complementary Split Ring Resonator (CSRR) antenna for the D-band demonstrates effective frequency band isolation and achieves proper impedance matching at 127.2 GHz and 137.8 GHz, respectively. The strong isolation between these two distinct frequency bands exhibited in the design antenna array ensures minimal interference and enhanced signal clarity.
- Our streamlined CSRR array design with two metallic layers (i.e., ground and patch) is shown to allow easy integration into PCBs and other compact electronic systems similar to a microstrip patch antenna.

The designed D-band antenna array, with dual resonant f quencies, offers advantages for 6G and beyond. By supporti dual-band functionality within a single antenna, it reduc the number of antennas required in Multiple Input Multi Output (MIMO) systems, leading to a more compact and co effective design. The dual-band makes the antenna ideal space-constrained devices and multiband system integrati [6]. The rest of this paper is organized as follows: the relat work in the domain of antenna design is discussed in Sec. Our designed antenna at D-band, including its geometry a working mechanism, is presented in Sec. III. Characterist of the dual-band array design are described in Sec. IV. Final the conclusion is drawn in Sec. V.

## II. Related Work

The efforts of antenna array design in the D-band have advanced significantly after decades-long development of integrated circuits, advanced materials, and prototyping methodology, among others. Most recently, an antenna in package (AiP) design in the D-band with dual-polarization is proposed in [7]. In particular, the wideband antenna array design uses a stub-loaded multi-layer and vertical power divider approach to achieve a bandwidth of more than 27 GHz with a return loss of $-10$ dB. In addition, patch antenna arrays, due to their compactness, are commonly used in various applications in both communications and sensing. In [8], a design of D-band $4\times4$ cavity-based patch antenna array is prototyped. This multi-layer design achieves a wide bandwidth of 20 GHz with an improved scanning range of $60^\circ$ in the azimuth plane. A 1600-element array operating at 150 GHz, achieving a peak gain of 32 dBi is presented by [9]. Similarly, a 1600-element array at 145 GHz, demonstrating a slightly higher peak gain of 33 dBi is proposed by [10]. Both designs employ three metallic layers as a part of their overall structure.

In terms of emerging stacked patch antenna designs, a dual-band resonance is achieved by a design of aperture-coupled stacked patch antenna in the frequency range of 90–128.5 GHz [11]. A flexible PCB has also been prototyped to demonstrate the wide bandwidth with almost 90% peak radiation efficiency. Others types of D-band antennas are designed and prototyped in recent years, which include on-chip antennas [12]–[14], hollow waveguide-based antenna arrays [15]–[17], and PCB-based antennas [18], [5], [19]. However, each comes with specific challenges, including intricate layers and low production cost efficiency, as aforementioned in Sec. I.

In the context of dual-band antenna designs, studies have been done on antenna operating at lower frequencies in the microwave spectrum. The design in [20] highlights the necessity of frequency band isolation between the 3.5 GHz and 4.85 GHz bands to mitigate performance degradation due to closely spaced antenna elements, a key challenge in modern mobile devices. A different approach focuses on a high isolation proximity-coupled multilayer patch antenna [6]. The authors address dual-frequency operation at 2.1 GHz and 2.45 GHz.

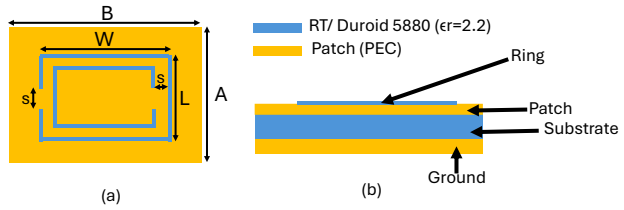


Fig. 1: Geometry and layers of the designed CSRR antenna. (a) Top view of CSRR. (b) The longitudinal cross-sectional view of the designed antenna shows the layered structure consisting of the ground plane, dielectric substrate, and radiating patch with etched dielectric rings, along with their respective material properties.

## III. Antenna Geometry and Working Mechanism

The primary objective of our design is to leverage the unique properties of complementary split ring resonators (CSRRs) to achieve frequency band isolation and proper impedance matching in high-frequency applications. CSRR antennas are designed similarly to patch antennas, especially considering their planar nature and fabrication process. CSRRs are often etched onto a substrate as planar structures, which allows them to be easily integrated into PCBs and other compact electronic systems like that of patch antenna [4]. This is advantageous over cavity-based or three-dimensional structures, which require more space.

### A. Geometry of Complementary Split Ring Resonator

The design of the proposed dual-band complementary split-ring resonator (CSRR) antenna is illustrated in Fig. 1. The CSRR antenna consists of a rectangular-shaped radiating patch incorporating two rectangular etched-out substrate rings, as shown in Fig. 1a. CSRR antenna is designed on an RT/Duroid 5880 substrate and the ground plane is positioned below the substrate as shown in Fig. 1(b). The radiating patch is fed by a microstrip line with an impedance of 50 $\Omega$. Antenna excitation is provided via a lumped port. The height of the substrate is selected within the range of $0.003\lambda \leq h_s \leq 0.05\lambda$ and the thickness of the patch should be very thin that is $t_h \ll \lambda$ as specified in [21, §14].

The width of the outer substrate ring, denoted as $W$, is calculated as [21]

$$W = \frac{c}{2f_r}\sqrt{\frac{2}{\varepsilon_r + 1}}, \tag{1}$$

where $c$ is the speed of light, $f_r$ is the operating frequency, and $\varepsilon_r$ is the dielectric constant of the substrate. The finite dimensions of the patch cause electric fields to extend beyond the physical boundaries of the patch. This effect, known as fringing, is influenced by the substrate's height $h_s$ and its dielectric constant $\varepsilon_r$ [21]. Due to fringing, the effective electrical length of the patch is greater than its physical length. The extended length is added to the physical length of the patch to obtain the effective length. This adjustment

ensures that the antenna resonates at the correct frequency, compensating for the fringing fields. The extended length denoted as $\Delta L$ is calculated using a very popular and practical approximate relation given as [21]

$$\Delta L = 0.412 h_s \frac{(\varepsilon_{\text{eff}} + 0.3)\left(\frac{W}{h_s} + 0.264\right)}{(\varepsilon_{\text{eff}} - 0.258)\left(\frac{W}{h_s} + 0.8\right)}, \quad (2)$$

where $h_s$ is the height of the substrate and $\varepsilon_{\text{eff}}$ is the effective dielectric constant, which plays a key role in determining extended length. It accounts for the non-uniform distribution of the electric field between the substrate and the surrounding air. As frequency increases, the effective dielectric c approaches the actual dielectric constant of the su indicating that more of the field is concentrated wit substrate. With condition $\frac{W}{h_s} > 1$, $\varepsilon_{\text{eff}}$ is given by [21

$$\varepsilon_{\text{eff}} = \frac{\varepsilon_r + 1}{2} + \frac{\varepsilon_r - 1}{2}\left(1 + \frac{12 h_s}{W}\right)^{-\frac{1}{2}}.$$

Finally, the length of the outer sub as [21]

$$L = \left(\frac{1}{2 f_r \sqrt{\varepsilon_{\text{eff}} \mu_0 \varepsilon_0}}\right.$$

where $\mu_0$ is the magnetic permeabil is the electric permittivity of free s impedance of a transmission line dep transmission line, $h_s$ and $\varepsilon_{\text{eff}}$ [21]. I transmission line is calculated to ach tics impedance. This width is used a for determining the strip width. It is to the slot width and the thickness o The dimension of the substrate m outer ring dimension in CSRR. Co dimensions are set to be twice that o compatibility and optimal performan

For our designed CSRR antenna, the outer ring are computed to be 0.671 mm in length, for an operating The antenna substrate features a th and a dielectric constant of 2.2. The i substrate and patch are double that o values of 1.67 mm for width and 1. thickness of rings, slot width, and stri to 0.11 mm. This slot width is subtracted from the outer ring's width and length to calculate the inner ring's dimensions. The ground and patch layers are modeled with a thickness of 0.002 mm, utilizing a perfect electric conductor for the simulation. The design parameters, specifically the width and length of the outer ring, the thickness of the ground plane and patch, and the slot width, are then adjusted to achieve a 50 Ω impedance at 142 GHz, thereby minimizing return loss. The CSRR antenna is designed and simulated using COMSOL Multiphysics and its RF module [22]. The final parameter values, post-optimization, are shown in Table I.

TABLE I: Design Parameters for CSRR Antenna

| Parameters | Value | Description |
|---|---|---|
| $f_r$ | 142 [GHz] | Operating frequency |
| $L$ | 0.683 mm | Length of outer ring |
| $W$ | 0.864 mm | Width of outer ring |
| $h_s$ | 0.06898 mm | Substrate thickness |
| $A$ | 1.35 mm | Length of substrate |
| $B$ | 1.65 mm | Width of substrate |
| $\lambda$ | 2.11 mm | Operating wavelength |
| $t_h$ | 0.002 mm | Thickness of metal and thickness of ground plane |
| $\varepsilon_r$ | 2.2 | Dielectric constant of substrate |
| $f_{\min}$ | 110 [GHz] | Minimum frequency |

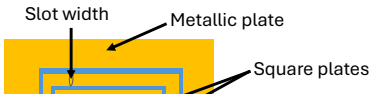


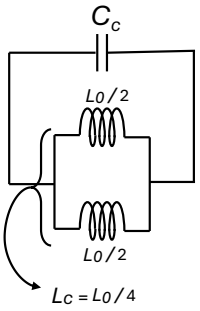


(b) Equivalent-circuit model.

Fig. 2: Topology of CSRR and its equivalent circuit model.

### B. Working Mechanism

Circuit theory provides a framework for representing complex electromagnetic structures using equivalent circuits. CSRR is modeled as $LC$ resonator and its resonant frequency $f_r$ is given by [23]

$$f_r = \frac{1}{2\pi\sqrt{L_c C_c}}, \quad (5)$$

where $C_c$ represents the capacitance between the square plates and the surrounding metallic plate, and $L_c$ is the inductance of the metallic strip connecting the square plates to the metallic plate. The value of $C_c$ is determined by the circumference of the square plates and the thickness of rings, while the inductance $L_c$ is influenced by the thickness of the rings and the strip width [24]. The circuit model of CSRR consists of the parallel combination of two inductances connecting the

two inner rings to the metallic plate which combined, is in series with a capacitance of rings as shown in Fig. 2b. Each inductance is given by $L_0/2$, where $L_0$ is the circumference of the ring per unit length inductance of the strip. The outer square plate is typically larger than the inner square plate as illustrated in Fig. 2a. Due to larger dimensions, the outer square plate contributes to a higher capacitance value, which corresponds to a lower frequency, given the inverse relationship between resonant frequency and capacitance in (5). Conversely, the inner square plate results in a lower capacitance value and a higher resonant frequency. This dual-band nature is a characteristic feature of CSRR [25].

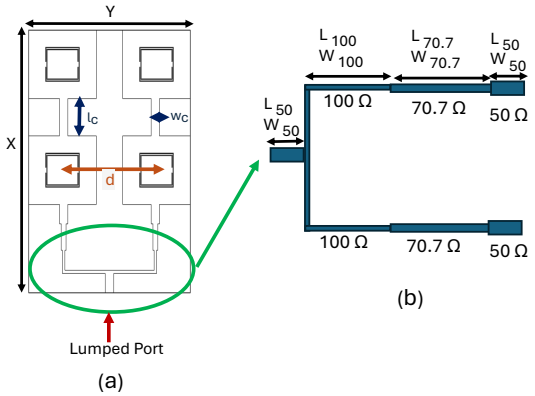


Fig. 3: Illustration of the designed dual-band 2×2 CSRR antenna array fed with T-junction equal power divider. (a) Geometry of the designed array in COMSOL simulation. (b) Layout of the T-junction equal power divider.

While a single antenna can serve dual-band purposes to a limited extent, array designs offer enhanced performance by utilizing multiple elements to optimize signal transmission and reception across two frequency bands. This section explores the methodologies guiding the design of dual-band CSRR array, emphasizing improved gain, and effective frequency isolation for modern communication systems. The design of the 2×2 series-fed CSRR array configuration is illustrated in Fig. 3. The element spacing in the array is half of the wavelength taken from the center of each element to avoid multiple maxima, aliasing, and causing nulls to be misplaced [21]. The patches are connected by the transmission line with dimensions of $l_c$ and $w_c$. The array is fed using a T-junction equal power divider as shown in Fig. 3b followed by a series-fed structure. This allows for a single feed input to all four elements. The T-junction power divider is selected because of its lossless characteristics arising due to the lack of resistive components compared to other types, such as the Wilkinson divider and resistive divider. The series-fed structure is chosen because it utilizes shorter transmission lines, thereby enhancing antenna efficiency. In contrast, the parallel-fed structure requires longer transmission lines, which can lead to spurious radiation and significant dielectric loss [26].

To ensure an equal power division between two antennas, a T-junction power divider with a quarter-wavelength transmission line configuration is designed in this work. The quarter-wavelength transformer formula is expressed as

$$Z_{\text{in}} = \frac{Z_0^2}{Z_L}, \tag{6}$$

where $Z_{\text{in}}$ is the input impedance, $Z_L$ is the load impedance and $Z_0$ is the characteristic impedance of the transformer. To ensure that $Z_{\text{in}}$ is equal to 50 Ω, the two paths branching from the input should collectively be a 50 Ω impedance. Given the 100 Ω segments in each path, using quarter-wavelength transformers can achieve the necessary impedance transformation with characteristics impedance of transformer as 70.7 Ω as deduced from (6). The operating frequency of our system is 142 GHz, and the corresponding wavelength is approximately 2.11 mm. Thus, the quarter-wavelength transformer is designed with a length of approximately 0.5278 mm. Using a quarter-wavelength segment with a characteristic impedance of 70.7 Ω, we transform the 100 Ω line impedance to match the 50 Ω load effectively.

The dimension of our designed CSRR array computed is 3.35×5.6627 mm$^2$. To improve the impedance matching between the connected patches, the width $w_c$ and the length $l_c$ of the transmission line are calculated for a 50 Ω microstrip line and optimized to be 0.7 mm and 1.2 mm respectively. The computed dimension of our designed array, including the dimension of our designed power divider is shown in Table II.

With the array geometry, the next step is to characterize the performance of the designed array. In practical antenna array design and simulation, proper meshing is crucial for efficient array characterization, especially in complex high-frequency applications. A well-defined mesh ensures that simulation results accurately reflect the real-world behavior of the antenna array by capturing detailed geometry and field variations. Proper mesh resolves small features and interactions between elements, which is essential for modeling radiation patterns and impedance characteristics. For the designed array, a physics-controlled mesh with an extra coarse element size is used in RF module of COMSOL Multiphysics [22].

## IV. Characterization of Dual-Band Array

Characterizing our dual-band array design focuses on several key parameters, including the far-field radiation pattern, array gain, directivity, bandwidth, and return loss. Specifically, the far-field radiation pattern of simulated 2×2 dual-band CSRR array is shown in Fig. 4, where the E-plane (shown as the blue solid curve) is defined by the direction of the dominant antenna polarization, and the H-plane (shown as the green dashed curve) is the plane in which the magnetic field is primarily polarized. The radiation pattern depicts the antenna array gain plotted in dB scale, which shows a maximum array gain of 13.8 dBi at 127.2 GHz and 14.8 dBi at 137.8 GHz. The realized gain of our array is 13.6 dBi at 127.2 GHz and 14.2

TABLE II: Design Parameters for 2×2 CSRR Antenna Array

| Parameters | Value | Description |
|---|---|---|
| $X$ | 5.6627 mm | Length of array |
| $Y$ | 3.35 mm | Width of array |
| $d$ | 1.6 mm | Element spacing |
| $l_c$ | 1.2 mm | Length of connecting link |
| $w_c$ | 0.7 mm | Width of connecting link |
| $L_{100}$ | 0.3983 mm | Length of 100 Ω microstrip line |
| $W_{100}$ | 0.06182 mm | Width of 100 Ω microstrip line |
| $L_{50}$ | 0.38611 mm | Length of 50 Ω microstrip line |
| $W_{50}$ | 0.2125 mm | Width of 50 Ω microstrip line |
| $L_{70.7}$ | 0.5278 mm | Length of quarter wavelength microstrip |
| $W_{70.7}$ | 0.12195 mm | Width of quarter wavelength microstrip |

dBi at 137.8 GHz. The calculated directivity of an array is 13.55 dB at 320° in the azimuth plane and 4° in the elevation plane for 127.2 GHz and 14.41 dB at 88° in the azimuth plane and 4° in the elevation plane for 137.8 GHz.

With the choice of the feed point in the design shown in Fig. 3(a), the return loss parameter ($S_{11}$) shown in Fig. 5 is less than $-10$ dB at 127.2 GHz and 137.8 GHz, respectively. The $-10$ dB $S_{11}$ operational bandwidth is 1.72 GHz (126.45 GHz–128.17 GHz) for the center frequency of 127.2 GHz and 2.45 GHz (136.55 GHz–139 GHz) for the center frequency of 137.8 GHz. The comparative analysis of various D-band antennas is presented in Table III. Our work uniquely combines array gain and frequency band isolation within a single-feeding topology, achieving comparable results to other designs while streamlining complexity. This highlights the effectiveness and efficiency of our approach to managing high-frequency signals, underscoring the innovation and practicality of our antenna design in the D-band spectrum.

## V. Conclusion

A design of a 2×2 dual-band CSRR antenna array for D-band frequencies is presented and characterized in this work. A key component of this design is the T-junction power divider with a quarter-wavelength section, which enables equal power division to the antenna element followed by a series-fed structure. The proposed antenna array design achieves a good band isolation between 127.2 GHz and 137.8 GHz, with 13.8 dBi and 14.8 dBi as maximum array gain at two resonating frequencies. This design shows its suitability for applications in next-generation wireless communication networks that require precise frequency separation and high antenna gain. Our future work will focus on extending the array dimension with more elements, enhancing operational bandwidth, and prototyping the antenna array to transition from simulation to practical experimentation, allowing for design validation and optimization opportunities.

## Acknowledgment

This material is based upon work supported by the National Science Foundation under Grant CNS-2216332, Grant CNS-2339811, and Grant CNS-2403286.

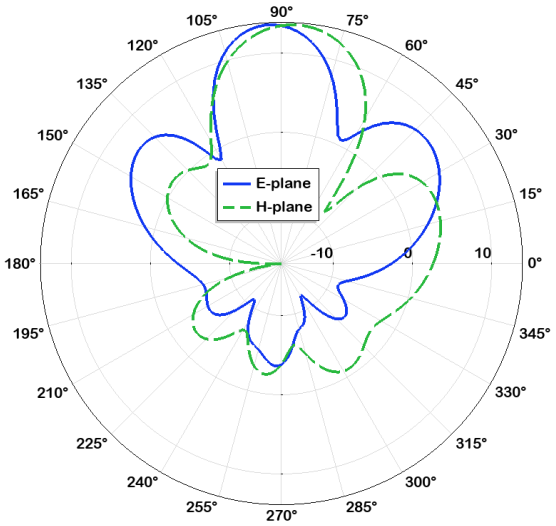


(a) 2-D pattern showing E-plane and H-plane at 127 GHz where peak gain computed is 13.8 dBi.

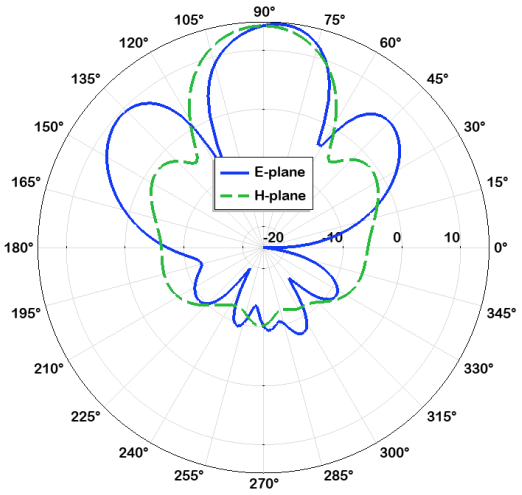


(b) 2-D pattern showing E-plane and H-plane at 137 GHz where peak gain computed is 14.8 dBi.

Fig. 4: Simulated 2-D far-field radiation pattern of dual-band 2×2 CSRR antenna array.

## References

[1] I. F. Akyildiz, C. Han, Z. Hu, S. Nie, and J. M. Jornet, "Terahertz band communication: An old problem revisited and research directions for the next decade," *IEEE Transactions on Communications*, vol. 70, no. 6, pp. 4250–4285, 2022.

[2] T. Maiwald, T. Li, G.-R. Hotopan, K. Kolb, K. Disch, J. Potschka, A. Haag, M. Dietz, B. Debaillie, T. Zwick, *et al.*, "A review of integrated systems and components for 6G wireless communication in the D-band," *Proceedings of the IEEE*, vol. 111, no. 3, pp. 220–256, 2023.

[3] J. M. Jornet, V. Petrov, H. Wang, Z. Popović, D. Shakya, J. V. Siles, and T. S. Rappaport, "The Evolution of Applications, Hardware Design,

D-band Antenna Array Designs

| Peak gain (dBi) | Number of metallic layers used | Height of Substrate (mm) |
|---|---|---|
| 13.8 dBi and 14.8 dBi | 2 | 0.06898 |
| 14 dBi | 4 | 0.255 |
| 32 dBi | 3 | 0.381 |
| 17.5 dBi | 6 | 0.32 |

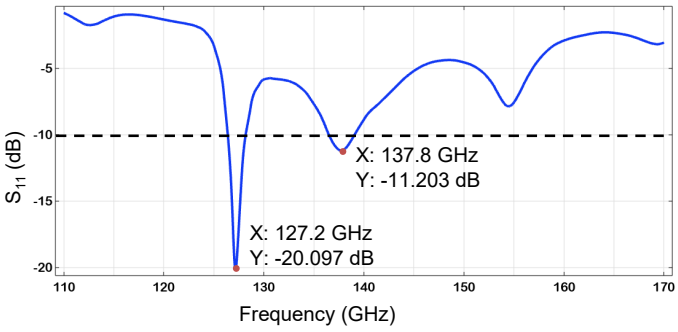


Fig. 5: Simulated $S_{11}$ of the dual-band 2×2 CSRR antenna array.


and Channel Modeling for Terahertz (THz) Band Communications and Sensing: Ready for 6G?," *Proceedings of the IEEE*, pp. 1–32, 2024.

[4] D. Zarifi, A. Farahbakhsh, and A. U. Zaman, "A gap waveguide-based D-band slot array antenna with interdigital feed network," *IEEE Transactions on Antennas and Propagation*, 2023.

[5] J. Xu, Z. N. Chen, X. Qing, and W. Hong, "140-GHz TE 20-mode dielectric-loaded SIW slot antenna array in LTCC," *IEEE Transactions on Antennas and Propagation*, vol. 61, no. 4, pp. 1784–1793, 2012.

[6] L. Inclan-Sanchez, J.-L. Vazquez-Roy, and E. Rajo-Iglesias, "High isolation proximity coupled multilayer patch antenna for dual-frequency operation," *IEEE Transactions on Antennas and Propagation*, vol. 56, no. 4, pp. 1180–1183, 2008.

[7] D. Jung, C.-J. Park, T. S. Kwon, J. W. Seo, B. Ahn, S.-H. Wi, and I. Na, "Terahertz Antenna-in-Package Design and Measurement for 6G Communications System," *IEEE Transactions on Antennas and Propagation*, vol. 72, no. 2, pp. 1085–1096, 2024.

[8] A. Lamminen, J. Säily, J. Ala-Laurinaho, J. de Cos, and V. Ermolov, "Patch antenna and antenna array on multilayer high-frequency PCB for D-band," *IEEE Open Journal of Antennas and Propagation*, vol. 1, pp. 396–403, 2020.

[9] W. Saleh, Y. Letestu, R. Sauleau, and E. M. Cruz, "Design and measurements of a high-performance wideband transmitarray antenna for D-band communications," *IEEE Antennas and Wireless Propagation Letters*, vol. 20, no. 9, pp. 1765–1769, 2021.

[10] F. F. Manzillo, A. Clemente, and J. L. González-Jiménez, "High-Gain $D$-Band Transmitarrays in Standard PCB Technology for Beyond-5G Communications," *IEEE Transactions on Antennas and Propagation*, vol. 68, no. 1, pp. 587–592, 2019.

[11] M. H. Maktoomi, Z. Wang, H. Wang, S. Saadat, P. Heydari, and H. Aghasi, "A Sub-Terahertz Wideband Stacked-Patch Antenna on a Flexible Printed Circuit for 6G Applications," *IEEE Transactions on Antennas and Propagation*, vol. 70, no. 11, pp. 10047–10061, 2022.

[12] Z.-C. Hao and J. Wang, "A D-band high-gain antenna for terahertz applications," in *2016 International Symposium on Antennas and Propagation (ISAP)*, pp. 546–547, IEEE, 2016.

[13] S. Pan and F. Capolino, "Design of a CMOS on-chip slot antenna with extremely flat cavity at 140 GHz," *IEEE Antennas and Wireless Propagation Letters*, vol. 10, pp. 827–830, 2011.

[14] R. Wang, Y. Sun, M. Kaynak, S. Beer, J. Borngräber, and J. C. Scheytt, "A micromachined double-dipole antenna for 122–140 GHz applications based on a SiGe BiCMOS technology," in *2012 IEEE/MTT-S International Microwave Symposium Digest*, pp. 1–3, IEEE, 2012.

[15] Y.-W. Wu, Z.-C. Hao, Z.-W. Miao, W. Hong, and J.-S. Hong, "A 140 GHz high-efficiency slotted waveguide antenna using a low-loss feeding network," *IEEE Antennas and Wireless Propagation Letters*, vol. 19, no. 1, pp. 94–98, 2019.

[16] M. M. Zhou and Y. J. Cheng, "D-band high-gain circular-polarized plate array antenna," *IEEE Transactions on Antennas and Propagation*, vol. 66, no. 3, pp. 1280–1287, 2018.

[17] D. Kim, J. Hirokawa, M. Ando, J. Takeuchi, and A. Hirata, "64*64-Element and 32*32-Element Slot Array Antennas Using Double-Layer Hollow-Waveguide Corporate-Feed in the 120 GHz Band," *IEEE Transactions on Antennas and Propagation*, vol. 62, no. 3, pp. 1507–1512, 2014.

[18] J. Xu, Z. N. Chen, X. Qing, and W. Hong, "140-GHz planar broadband LTCC SIW slot antenna array," *IEEE Transactions on Antennas and Propagation*, vol. 60, no. 6, pp. 3025–3028, 2012.

[19] J. Xiao, X. Li, Z. Qi, and H. Zhu, "140-GHz $TE\_\{340\}$-mode substrate integrated cavities-fed slot antenna array in LTCC," *IEEE Access*, vol. 7, pp. 26307–26313, 2019.

[20] "Isolation enhancement in dual-band monopole antenna for 5G applications, author=Wang, Wen and Wu, Yongle and Wang, Weimin and Yang, Yuhao," *IEEE Transactions on Circuits and Systems II: Express Briefs*, vol. 68, no. 6, pp. 1867–1871, 2020.

[21] C. A. Balanis, *Antenna theory: analysis and design*. John wiley & sons, 2016.

[22] COMSOL, Inc, *RF Module User's Guide, version 6.2*, 2023.

[23] Y. Dong, H. Toyao, and T. Itoh, "Design and characterization of miniaturized patch antennas loaded with complementary split-ring resonators," *IEEE Transactions on antennas and propagation*, vol. 60, no. 2, pp. 772–785, 2011.

[24] A. Ebrahimi, W. Withayachumnankul, S. F. Al-Sarawi, and D. Abbott, "Compact dual-mode wideband filter based on complementary split-ring resonator," *IEEE Microwave and Wireless Components Letters*, vol. 24, no. 3, pp. 152–154, 2013.

[25] J. D. Baena, J. Bonache, F. Martín, R. M. Sillero, F. Falcone, T. Lopetegi, M. A. Laso, J. Garcia-Garcia, I. Gil, M. F. Portillo, *et al.*, "Equivalent-circuit models for split-ring resonators and complementary split-ring resonators coupled to planar transmission lines," *IEEE transactions on microwave theory and techniques*, vol. 53, no. 4, pp. 1451–1461, 2005.

[26] M. Khalily, R. Tafazolli, T. A. Rahman, and M. R. Kamarudin, "Design of Phased Arrays of Series-Fed Patch Antennas With Reduced Number of the Controllers for 28-GHz mm-Wave Applications," *IEEE Antennas and Wireless Propagation Letters*, vol. 15, pp. 1305–1308, 2016.

[27] T. Dao, A. Kearns, D. R. Paredes, and G. Hueber, "Wideband High-Gain Stacked Patch Antenna Array on Standard PCB for D-Band 6G Communications," *IEEE Antennas and Wireless Propagation Letters*, 2023.